PROCEEDINGS, Thirty-Eighth Workshop on Geothermal Reservoir Engineering
Stanford University, Stanford, California, February 11-13, 2013
SGP-TR-198

DENSITY DRIVEN (INCLUDING GEOTHERMAL EFFECT) NATURAL CONVECTION OF CARBON DIOXIDE IN BRINE SATURATED POROUS MEDIA IN THE CONTEXT OF GEOLOGICAL SEQUESTRATION

*Akand W. ISLAM, **Muhammad A. R. SHARIF, *Eric S. CARLSON

*Department of Chemical & Biological Engineering
**Department of Aerospace Engineering & Mechanics
The University of Alabama
Tuscaloosa, AL 35487, USA
e-mail: awislam@crimson.ua.edu

ABSTRACT

Double diffusive natural convection of carbon dioxide in two-dimensional cavities filled with brine saturated porous media is numerically investigated in this study. Vertical gradients of carbon dioxide concentration and temperature are imposed across the height of the cavity. The objective is to understand the dissolution of carbon dioxide through natural convection process over long period of time after sequestration into subsurface porous media aquifer. The problem parameters are the solutal Rayleigh number ($100 \leq Ra_s \leq 10000$), the buoyancy ratio ($2 \leq N \leq 100$), the thermal Rayleigh number ($2 \leq Ra_T \leq 100$), the cavity aspect ratio ($0.5 \leq A \leq 2$), and a fixed Lewis number ($Le = 301$). It is found that the CO_2 plumes move faster when Ra_s is increased, however slow down with decreasing N. For every simulation run, the average CO_2 dissolution ($\bar{S} = \frac{\sum_{i}^{n_i}\sum_{j}^{n_j} c_{i,j}}{n_i \times n_j}$) in the reservoir is computed. At early stage ($\leq$10 years) of the convection process, the CO_2 dissolutions are same for all cases studied. After 500 years the dissolution is found to be around 0.63 for $N = 100$, and around 0.47 for $N = 2$, respectively. After 2000 years the dissolution rate is extremely slow. When the reservoir aspect ratio (A) is changed, the dissolution rate changes slightly. The rate is slightly higher in laterally wide reservoir, which makes it better candidate than the deeper aquifer from the context of CO_2 sequestration.

INTRODUCTION

In order to control carbon emissions, the use of technologies to capture and store CO_2 has rapidly emerged as an important physically and economically viable method these days. Various CO_2 storage methods in geological formations, such as depleted oil and gas fields, un-mineable coal seams, saline-filled basalt formations, etc., have been suggested. This process promises to reduce the cost of achieving considerable reductions in CO_2 emissions over the next few decades (Hassanzadeh et al., 2005a). Geological storage in underground saline formation involves injecting supercritical CO_2 at high pressure into a saline aquifer capped by a rock formation. Following injection, CO_2 is accumulated between the cap and aquifer surface. Eventually, the CO_2 is trapped by two different mechanisms, namely; capillary trapping and solubility trapping. In capillary trapping, part of the CO_2 rises through porous rock formation above due to buoyancy and capillary forces and gets trapped into the rock pores. On the other hand, at the interface between the CO_2-rich

phase and brine (Farajzadeh et al., 2009), dissolution of CO_2 into brine starts by molecular diffusion increasing the brine density (Islam and Carlson, 2012) (by about 1%) on the aquifer top surface which then sinks down into the brine by natural convection due to solute gradient. This phenomenon is termed as solubility trapping. Another destabilizing agent is the naturally occurring geothermal temperature gradient (typically ~3 °C/100 meter depth), which induces some sort of upward natural convection of the brine. The interaction of these two opposing processes, termed as double diffusive transport, determines the resultant rate of dissolution/deposition of the CO_2 in the brine. The geothermal gradient is partially compensated by the geo-pressure gradient (Lindeberg and Wessel-berg, 1997) (normally ~10 bar/100 meter depth). The convective mixing enhances dissolution of CO_2 through continuously removing CO_2-rich brine from the top layer and bringing under-saturated brine into contact with the downward advancing CO_2 plume. For the design, operation, and maintenance of such a geologic CO_2 storage facility, it is very important to quantify the rate of dissolution and understand the transport mechanism. The time scale of the solubility trapping is very large ranging hundreds to thousands of years during which the high pressure free phase CO_2, accumulated between the aquifer free surface and the top rock formation may leak out through rock fractures (Hassanzadeh et al., 2005b). The chance of leaking reduces when a significant amount of CO_2 dissolves into the brine.

Comprehensive investigations have been carried out on double-diffusive convection where heat and solute are the diffusive components (Oldenburg and Pruess, 1998; Stern, 1975). An extensive work has been done in the context of porous media, especially related to the environmental problems and the transport of contaminants (Cooper et al., 1997; Green, 1984; Mojtabi et al., 2005; Poulikakos, 1986). Studies investigating stability analysis for the onset time for convection, the preferred wavelength for the growth of convective fingers, growth rates, and solutal and thermal effects have also been published (Bhadauria, 2006; Javaheri et al., 2010; Poulikakos, 1986; Sodha and Kumar, 1985). The extensive time scale of the storage process operation renders the experimental investigation of the process impractical. The viable alternative is to study the double diffusive process numerically, which is the motivation behind this work. The use of modeling and simulation to make predictions on the timescale is obviously impossible to validate, since even in a field operation one cannot history match more than a small amount of the relevant time period (Ennis-King and Paterson, 2003).

In this paper the double-diffusive convection of CO_2 in brine under vertical thermal and solutal gradients is numerically studied considering reservoir conditions suitable to geologic sequestration. Realistic simulation inputs, obtained through extensive literature review, are provided for the computations. Results are presented graphically in terms of the propagation of the CO_2 front through the aquifer with time for various cavity configurations ($0.5 \leq A \leq 2$) and for a range of the solutal Rayleigh number ($100 \leq Ra_s \leq 10000$) and thermal Rayleigh number ($2 \leq Ra_T \leq 100$). The effects of variation of these geometric and hydrodynamic parameters on the CO_2 front propagation and dissolution are analyzed and evaluated.

DESCRIPTION OF THE PROBLEM AND GOVERNING EQUATIONS

The geometry under consideration is a two-dimensional rectangular cavity reservoir, sketched in **Figure 1**, filled with porous medium saturated with brine (H_2O+NaCl), with a height H and length L. The permeability of the porous medium is φ. Initially the fluid is at rest and there is no

CO_2 dissolved. Boundary conditions are no fluid flow across all boundaries and no solute fluxes across lateral and bottom boundaries at all time. Also there is no heat flux across the lateral boundaries while the top and bottom boundaries are maintained at isothermal cold and hot temperatures, respectively. We assume that CO_2-liquid interface is relatively sharp and fixed at the top boundary; meaning pressure change due to dissolution is negligible. This approximation is reasonable below a depth of 1000 m which is the usual case of geological sequestration (Ennis-King and Paterson, 2005). The brine is initially quiescent and the medium is homogeneous in terms of porosity and permeability. The presence of a capillary transition zone between the gas and the brine phase is disregarded. Therefore only the liquid phase is modeled and the presence of the gas phase at the top is represented by a boundary condition for the liquid phase. The Boussinesq approximation and Darcy flow model are assumed valid. Moreover, we assume that velocity-based dispersion and capillary effects are negligible and that geochemical reactions are not occurred. We only expect a laminar flow regime since Rayleigh number is low. Boundary conditions for the temperature are opposite to concentration, because the geo-temperature at the bottom of the reservoir is higher than that at the top, the actual temperature difference varies from place to place. The density gradient owing to concentration and temperature variations are the source of natural convection here. For such a system, the governing equations of flow and concentration field are:

(a) Continuity equation

$$\frac{\partial \rho}{\partial t}+\frac{\partial\left(\rho u_x\right)}{\partial x}+\frac{\partial\left(\rho u_z\right)}{\partial z}=0 \qquad (1)$$

(b) Darcy's law

$$u_x=-\frac{k}{\mu}\frac{\partial p}{\partial x}, \qquad (2)$$

$$u_z=-\frac{k}{\mu}\left(\frac{\partial p}{\partial z}-\rho g\right) \qquad (3)$$

(c) Concentration transport equation

$$\frac{\varphi \partial c}{\partial t}+u_x\frac{\partial c}{\partial x}+u_z\frac{\partial c}{\partial z}=\varphi D\left(\frac{\partial^2 c}{\partial x^2}+\frac{\partial^2 c}{\partial z^2}\right) \qquad (4)$$

(d) Energy equation:

$$\rho_0 C_p\left(\frac{\partial T}{\partial t}+u_x\frac{\partial T}{\partial x}+u_z\frac{\partial T}{\partial z}\right)=\kappa\left(\frac{\partial^2 T}{\partial x^2}+\frac{\partial^2 T}{\partial z^2}\right) \qquad (5)$$

For small density variations due to temperature and concentration changes at constant pressure, the brine density is a linear function of temperature and concentration of solute as given by

$$\rho=\rho_0\left[1+\beta_c\left(c-c_0\right)+\beta_T\left(T-T_0\right)\right] \qquad (6)$$

where

$$\beta_c=\frac{1}{\rho_0}\left[\frac{\partial \rho}{\partial c}\right]_T \quad \text{and} \quad \beta_T=\frac{1}{\rho_0}\left[\frac{\partial \rho}{\partial T}\right]_c \qquad (7)$$

and we obtain

$$\frac{\partial \rho}{\partial x}=\rho_0\left[\beta_c\frac{\partial c}{\partial x}+\beta_T\frac{\partial T}{\partial x}\right] \qquad (8)$$

After eliminating the pressure by cross-differentiation of equations (2) and (3) we get

$$\frac{\partial u_z}{\partial x}-\frac{\partial u_x}{\partial z}=\frac{kg\rho_0}{\mu}\left[\beta_c\frac{\partial c}{\partial x}+\beta_T\frac{\partial T}{\partial x}\right] \qquad (9)$$

The equations to be solved are Eqs. (1), (4), (5), and (9) to obtain u_x, u_z, c and T.

Dimensionless form of the equations

Considering the cavity height, H, as the characteristic length and $\varphi D/H$ as the characteristic velocity following dimensionless variables are defined,

$$x^* = \frac{x}{H},\ z^* = \frac{z}{H},\ u_x^* = \frac{Hu_x}{\varphi D},\ u_z^* = \frac{Hu_z}{\varphi D},\ \psi^* = \frac{\psi}{\varphi D}$$

$$t^* = \frac{Dt}{H^2},\ c^* = \frac{c - c_r}{c_0 - c_r},\ T^* = \frac{T - T_r}{T_0 - T_r},\ u_x^* = -\frac{\partial \psi^*}{\partial z^*},\ u_z^* = \frac{\partial \psi^*}{\partial x^*}$$

$$Ra_s = \frac{\Delta\rho_c gkH}{\varphi D\mu},\ Ra_T = \frac{\Delta\rho_T gkH}{\mu\alpha},\ Le = \frac{\alpha}{\varphi D}.$$

After applying the Boussinesq approximation the final forms of dimensionless equations are

$$\frac{\partial^2 \psi^*}{\partial x^{*2}} + \frac{\partial^2 \psi^*}{\partial z^{*2}} = Ra_s \left(\frac{\partial c^*}{\partial x^*} - \frac{1}{N} \frac{\partial T^*}{\partial x^*} \right) \qquad (10)$$

$$\frac{\partial c^*}{\partial t^*} + u_x^* \frac{\partial c^*}{\partial x^*} + u_z^* \frac{\partial c^*}{\partial z^*} = \frac{\partial^2 c^*}{\partial x^{*2}} + \frac{\partial^2 c^*}{\partial z^{*2}}. \qquad (11)$$

$$\frac{\partial T^*}{\partial t^*} + \varphi u_x^* \frac{\partial T^*}{\partial x^*} + \varphi u_z^* \frac{\partial T^*}{\partial z^*} = \frac{1}{\mathrm{Pr}} \left(\frac{\partial^2 T^*}{\partial x^{*2}} + \frac{\partial^2 T^*}{\partial z^{*2}} \right) \qquad (12)$$

where $N = -\dfrac{\beta_c \Delta c}{\beta_T \Delta T}$ is the buoyancy ratio and $\mathrm{Pr} = \dfrac{\rho_0 c_p D}{\kappa}$.

Boundary and initial conditions

The initial condition is,

$$\text{at } t^* = 0 \ \ \psi^* = 0,\ c^* = 0, T^* = 0. \qquad (13)$$

The boundary conditions are shown in **Figure 1**,

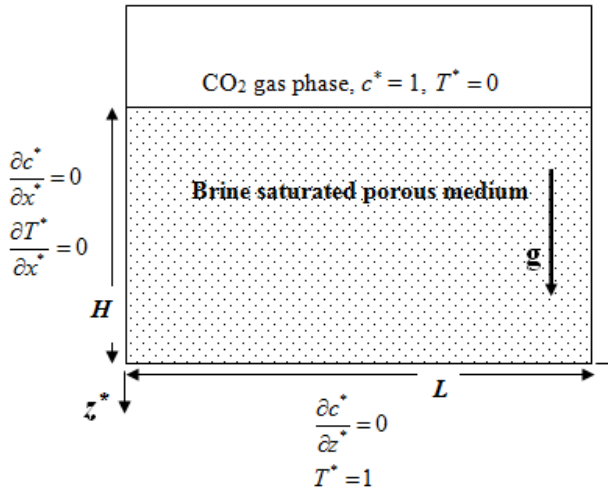

Figure 1: Schematic diagram of our hypothetical reservoir model

NUMERICAL METHOD

Numerical simulation of density-driven transport problem is very sensitive to discretization errors. The following criteria must be fulfilled for the stability of the transport equations given by

$$\frac{u^* \Delta t^*}{\varphi \Delta x^*} \le \frac{P_E}{2} \qquad (14)$$

where $P_E = \dfrac{u^* \Delta x^*}{D\varphi}$. The simulation was performed with 81×81 uniform rectangular grid cells for the cavity with aspect ratio of unity, and time step (Δt^*) was taken as 10^{-6} (equivalent to ~29 days based on H = 100 m) to meet above conditions. A sequential solution procedure was used to solve the elliptic Poisson equation (10) and the concentration and temperature transport equations (11) and (12). Equation (10) is solved by Point Gauss-Sidel iterative method with convergence criteria of $\sum abs\left(\frac{\psi^{i+1} - \psi^i}{\psi^i}\right) < 10^{-6}$ where the superscript i denotes iteration step number. Equations (11) and (12) are solved using the Alternating Direction Implicit (ADI) method where the convection terms are discretized using the upwind differencing and the diffusion terms are discretized using the central differencing. The developed code prediction for natural convection in a cavity was checked against the literature benchmark solutions (Hassanzadeh et al., 2005a; Simpson and Clement, 2003) and the results are in satisfactory agreement with the published simulations independent of the number of grid cells. It is required that the interface concentration be perturbed in order to observe the downward propagation of the finger like concentration fronts. Therefore a sinusoidal perturbation is used on the top interface in the form

$$c^*(x^*, z^* = 0, t^* = 0) = 1 + 0.01 \sin(2\pi n x^*) \qquad (15)$$

where the wave number (n) of 24 is used. Basically the long term behavior is not dependent on the initial perturbation (Farajzadeh et al. 2007). Moreover, the growth of the perturbations is a weak function of the wavelength. Pore-level perturbations and thermo-mechanical fluctuations cause the perturbation to start the finger like plumes in reality (Gunn and Krantz, 1980; Landau and Lifshitz, 1969)Pore-level instabilities (Yortsos et al., 1997) is ignored here, however.

The important assumptions in this study are the homogeneity and isotropy of the porous medium. The effect of velocity-induced dispersion is ignored and the flow field as single-phase is considered. Additionally other mechanisms like, precipitation and geochemical reactions are not accounted for simplicity.

RESULTS AND DISCUSSIONS

The double diffusion is imposed here through the buoyancy ratio (N) which was varied between 2 and 100. This represents vast differences of geothermal gradients. The geothermal gradient is not same everywhere; for instance, very high gradient can be observed as 20 °C/100 m at the Mid-Atlantic Rift, whereas in Iceland there is almost no gradient (~ 0 °C/100 m) (Lerner and Lerner, 2003). The direction of the flow due to thermal buoyancy forces is anticlockwise because temperature at the bottom of the reservoir is always higher than at the top. On the other hand, the flow owing to concentration gradient is clockwise, opposing the thermal flow. The solutal Rayleigh number, Ra_s, is varied from 100 – 10,000. The porosity (φ) of a typical reservoir (Oldenburg and Pruess, 1998), of 0.30, and recently reported (Newell et al., 2011) diffusion coefficient (D) of brine filled porous media, of 4×10^{-9} m^2/s, respectively, are taken for calculations. In order to calculate the Prandtl number, Pr, in the energy equation, the required inputs are collected from Sharqawy et al (Sharqawy et al., 2010). Pr is calculated to be as 0.0062. To understand the natural convection of different reservoir shapes, the aspect ratio (A) is varied 0.5, 1, and 2 representing deep, square, and, shallow reservoir configurations, repectively. The thermal diffusivity (α) is considered constant assigning the value 3.7×10^{-7} m^2/s (Javaheri et al., 2010). Hence, the Lewis number, Le, is fixed at 310. To discuss the results in terms of a combination of the solutal Rayleigh number, Ra_s, and the buoyancy ratio, N, the equivalent Rayleigh number, Ra_e, expressed as

$$Ra_e = Ra_s\left(1+\frac{1}{N}\right) \quad (16)$$

is introduced.

Effects of Ra_s and N

First, various scenarios of varying Ra_s from low (100) to relatively high (10,000) and N from 2 to 100 for the case of A = 1 (square shape) are discussed. **Figure 2** shows the concentration distribution for Ra_s = 100 and N = 100 where only the top side of the vertical domain is zoomed out. The corresponding Ra_e for this case is 99. By definition [Equation (16)] Ra_e does not change significantly unless N is low and close to 1. Equation (16) also implies that when the buoyancy ratio is higher, the thermal effect on CO_2 dissolution is relatively minor. When Ra_e is low (such as 99), even though the induced perturbations at the top interface initiate very tiny convection cells, they cannot survive as the time marches. For low Ra_e the dissolution is completely diffusion dominated and therefore propagation of CO_2 concentration front into brine is extremely slow. This is unfavorable because in such case CO_2 will have to be trapped over the aquifer for a very long time (thousands of years) and may caveat leakage through any fracture in the top rock formations. Average dissolution (or

concentration) of CO_2 in the model reservoir is defined as

$$\bar{S} = \frac{\sum_{i}^{n_i}\sum_{j}^{n_j} c_{i,j}}{n_i \times n_j} \qquad (18)$$

After about 4 years the average dissolution is found to be 0.016 while after 100 years that is 0.046. After 500 years the average dissolution of CO_2 in the aquifer will be only 0.094. During early periods, CO_2 dissolves in the brine slowly and as time passes the diffusion dominated dissolution rate is slightly enhanced.

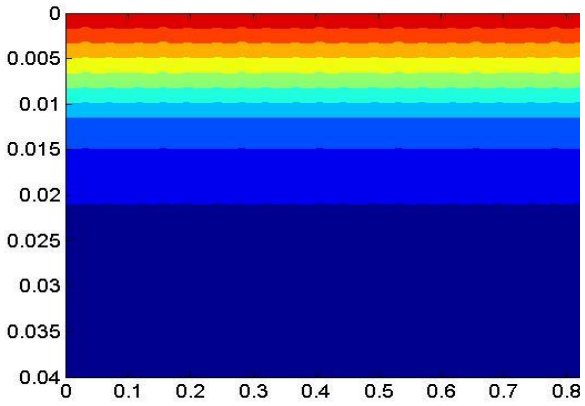

(a)

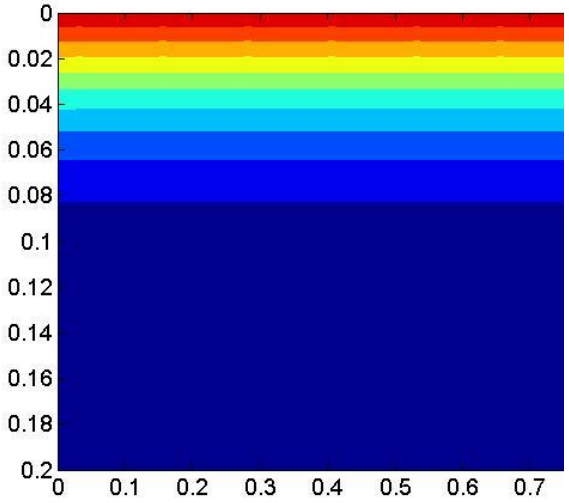

(b)

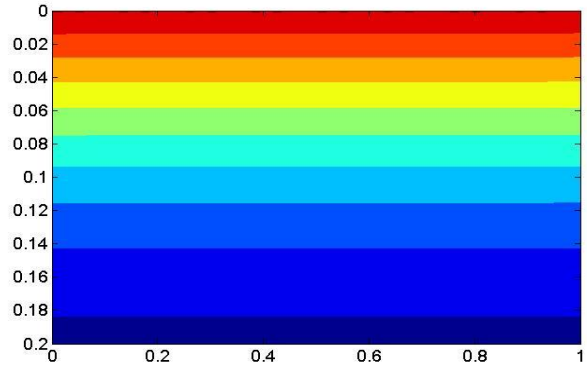

(c)

Figure 2: Concentration profiles for Ra_s = 100, N = 100, at (a) t = 4, (b) t = 100, and (c) t = 500 years.

When N is decreased to 50, the Ra_e becomes 98 and correspondingly produces almost the same concentration distribution for Ra_e = 99 as shown in **Figure 2**. When the thermal buoyancy effect is increased by substantially decreasing N (= 2), the Ra_e decreases to 50. At this low equivalent Rayleigh number, CO_2 dissolution rate is extremely slow (not shown).

The CO_2 propagation over the time is shown in **Figure 3** when Ra_s is increased to 1,000 with N = 100 producing Ra_e of 990. In this case we see that, even up to 100 years the concentration front propagation is primarily diffusive and therefore the average dissolution reaches to only 0.05. However, after long time, the convective mixing becomes traceable. **Figure 3c** shows CO_2 concentration fingers after 500 years and some of them reach around half of height of the reservoir producing average dissolution of 0.15. Since initial perturbations of the wavelength of 24 were introduced, convection cells start to evolve in 23 segments and they merge together as the fluid convection becomes stronger. Nevertheless, some fingers grow faster than the others and the finger wavelength increases due to random but stronger

nonlinear interactions. It is also observed that the CO_2 finger front movement is relatively faster close to the sidewalls than the central region. Decreasing the value of N to 50 exhibits marginal difference (Ra_e = 980), and is not shown separately. Further decrease of N to 2 decreases the equivalent Rayleigh number to 500 which basically shows only diffusion even after 500 years (not shown here). Although the interface is perturbed, the imposed initial disturbances are damped and the CO_2 front advance as diffusion like manner.

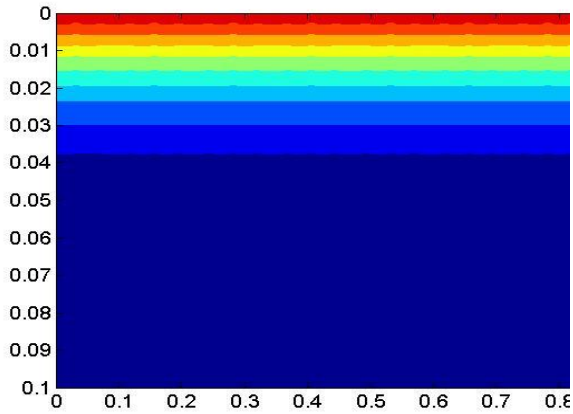

(a)

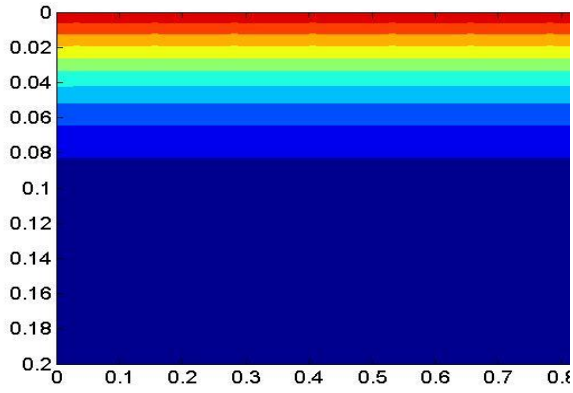

(b)

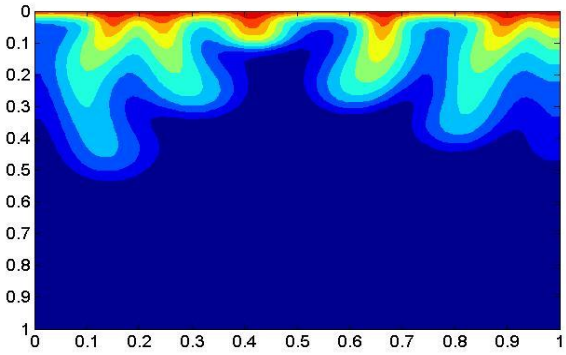

(c)

Figure 3: Concentration profiles for Ra_s = 1000, N = 100, at (a) t = 20, (b) t = 100, and (c) t = 500 years.

For the case of Ra_s = 10,000 and N = 100 (Ra_e = 9,900), **Figure 4** shows the CO_2 concentration distribution at several time periods. Here the Ra_s is high enough to instigate natural convection even at early periods. Small convection cells are clearly seen in **Figure 4a** after the simulation is run up to 4 years. At this time, the average concentration is 0.02. The CO_2 concentration is distributed more evenly as time elapses. The 23 fingers generated initially reduce to 8 after 10 years with a corresponding dissolution of 0.03. The fingers keep moving downward dissolving more CO_2 in brine ($\bar{S} = 0.07$ after 20 years). Many of the fingers are observed to undergo strong interactions while others are in the process of being faded. When the CO_2 front first reaches to the bottom of the reservoir (after 68 years) only one isolated big central plume survives, while two other fingers on both sides of the central plume, originating from single feeding site on top, are still in competition. Dynamics of the fluid movements becomes irregular. As the time passes new feeding sites appear and the older ones are banished. In other regions, multiple fingers can attach to a single feeding site, a process which is governed by diffusion. The non-linear dynamics then

selects one over the others as the favorable flow path (Riaz et al., 2006). This is noteworthy that the merging process starts at the stem sides rather than at the tip of the fingers and from there they spread to the rest of the system.

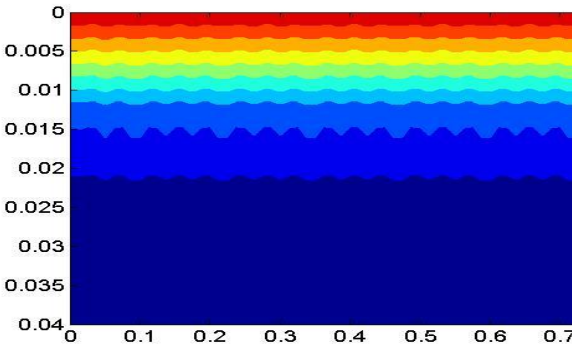

(a)

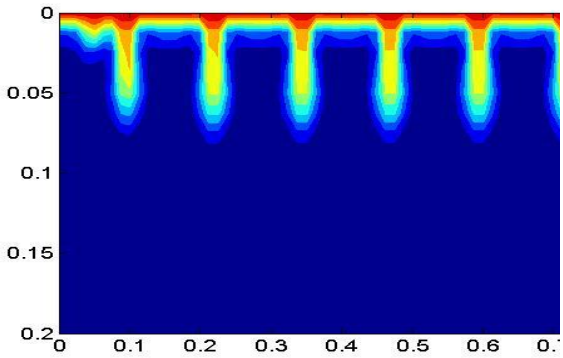

(b)

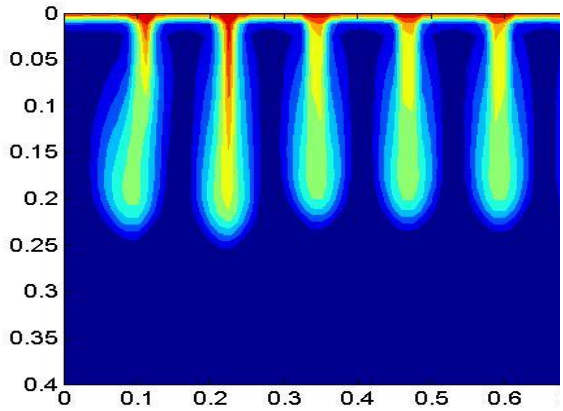

(c)

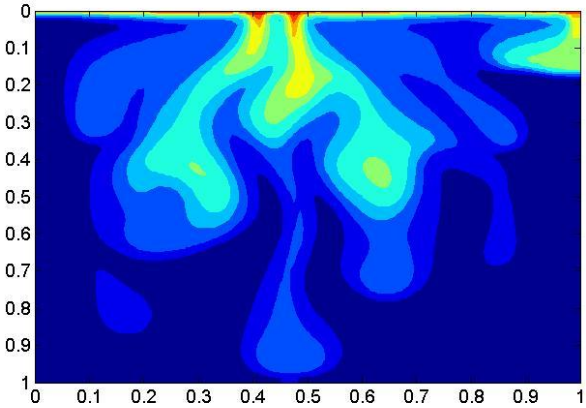

(d)

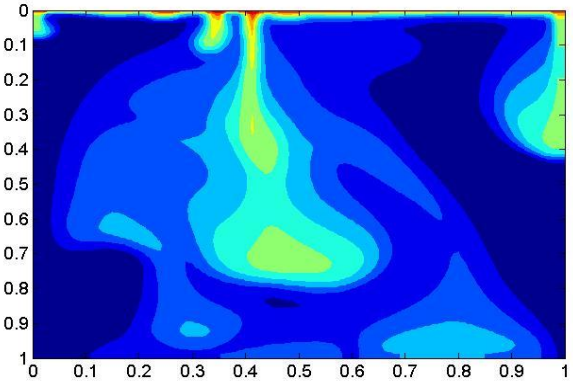

(e)

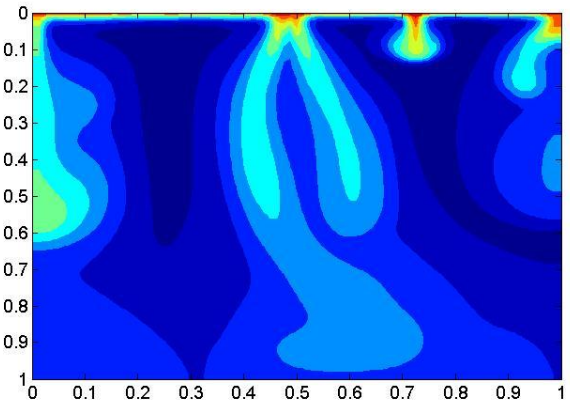

(f)

Figure 4: Concentration profiles for Ra_s = 10000, N = 100, at (*a*) t = 4, (*b*) t = 10, (*c*) t = 20, (*d*) t = 68, (e) t = 100, and (*f*) t = 500 years.

The larger fingers travel with less interactions with the neighboring fingers. Moreover, large fingers are connected to the thin diffusive shear layer at discrete locations serving as the feeding sites of high-density fluid for the fingers. The animation of the transient advancement of the plumes at Ra_e = 9,900 may be watched at the website (http://www.youtube.com/watch?v=oyUNj7HEaro). Though CO_2 reaches at the bottom relatively early, the saturation is below 0.20. **Figure 4f** shows simulation results for 500 years. The later stage behavior of the convection process cannot be ascertained from the results of early stage and the prediction of the rate of dissolution is very complex. Porosity, permeability, density difference, temperature difference, etc. are the factors which all are retained in the Rayleigh number and therefore the complexity in the flow behavior is strongly dependent on this Rayleigh number (both solutal and thermal). It is already apprehended that the concentration front spreads faster for larger equivalent Rayleigh number. Average dissolution of CO_2 in the reservoir after 100 and 500 years is 0.21 and 0.62, respectively for N = 100. When N is reduced to 2, these corresponding dissolutions are 0.16 and 0.47, respectively. The concentration contours of this case (N = 2) are shown in **Figure 5**. At early stages CO_2 dissolutions are same (~0.02) for both N = 100 and 2. This is because at the early stages the transport process is mostly diffusion dominated. As mentioned earlier, the CO_2 front reaches the bottom of the aquifer after 68 years when N = 100 while the front advances little more than half of the reservoir depth for N = 2 even after 100 years.

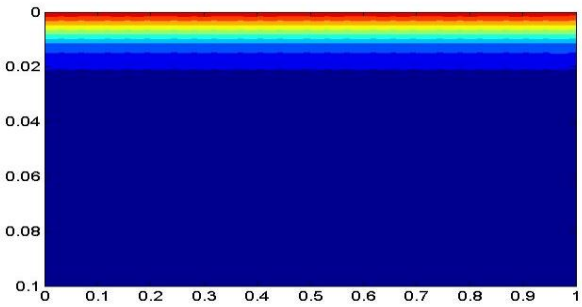

(a)

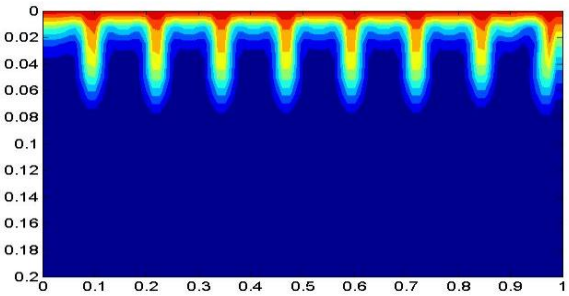

(b)

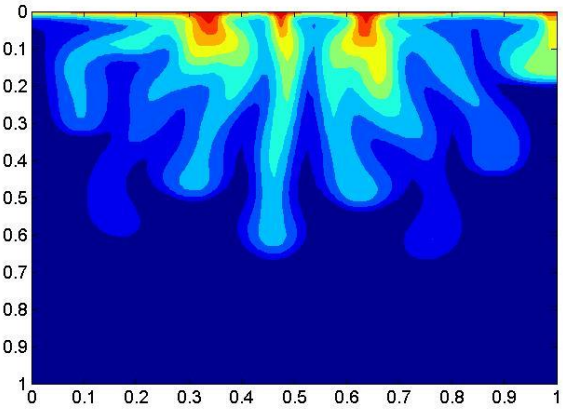

(c)

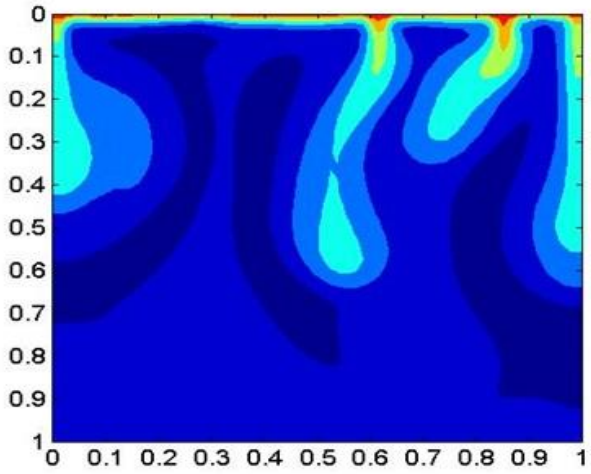

(d)

Figure 5: Concentration profiles for Ra_s = 10,000, N = 2, at (a) t = 4, (b) t = 20, (*c*) t = 100, (*d*) t = 500 years.

Effects of A

In order to understand the effects of reservoir aspect ratio on the transport process additional computations are performed for A = 0.5 (laterally wide) and A = 2 (deep well). At early stages (< 20 years), the diffusion dominated average dissolution of CO_2 are almost same ($\bar{S}$ ~ 0.02 after 4 years and 0.07 after 20 years) for any aspect ratio while at later stages (> 100 years) the average dissolution varies slightly with aspect ratio. **Figure 6** shows the evolution of the CO_2 concentration front with time for Ra_s = 10,000, N = 100, and A = 0.5. The CO_2 distribution after 100 years is very uneven.

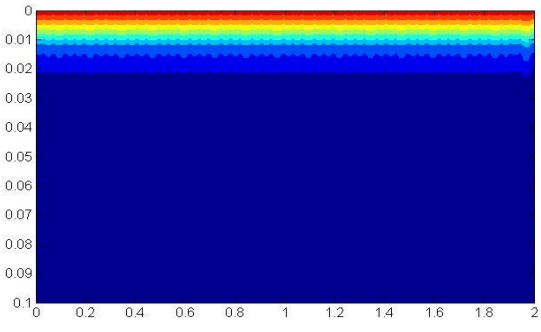

(a)

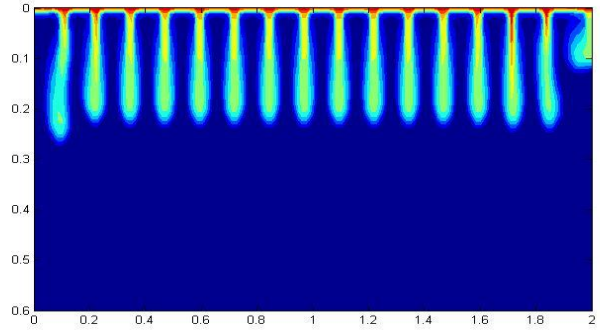

(b)

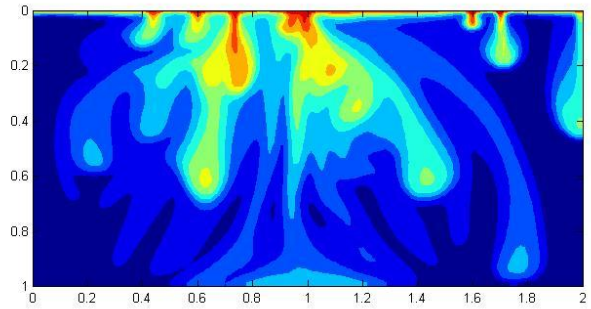

(c)

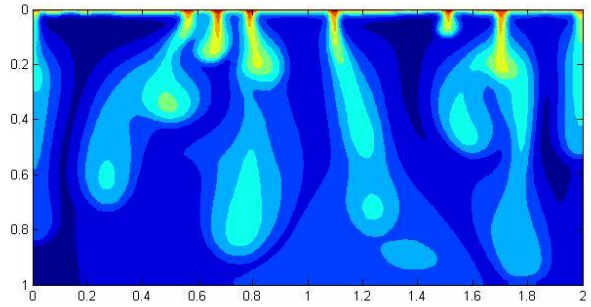

(d)

Figure 6: Concentration profiles for Ra_s = 10,000, N = 100, A = 0.5, at (a) t = 4, (b) t = 20, (c) t = 100, (d) t = 500 years.

Interestingly, the mixing is very slow near the side walls. It is also noted that the reservoir aspect ratio has little effect on the CO_2 dissolution. When the thermal effect is made significant by decreasing N to 2, the

concentration distribution obtained at 100 and 500 years are shown in **Figure 7.** Unlike for N = 100, the mixing seems even and almost symmetrical about the vertical midline at 100 years. In this case, the increased thermal effect counteracts with the solutal buoyancy effects making the dissolution process slower. Therefore the average dissolution is low (0.17). Over time the front propagation accelerates little more resulting in average dissolution 0.48 after 500 years.

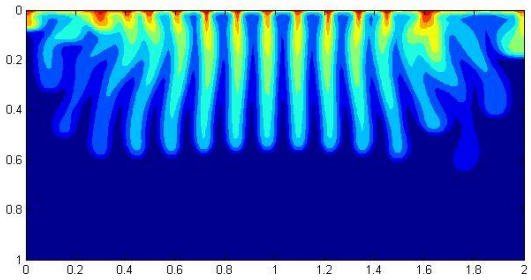

(a)

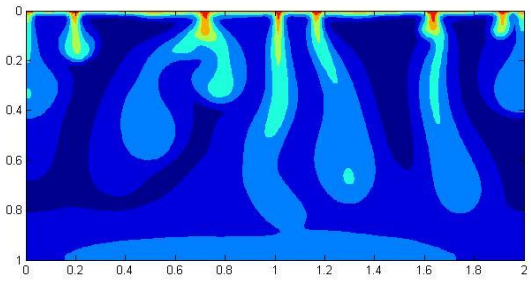

(b)

Figure 7: Concentration profiles for Ra_s = 10000, N = 2, A = 0.5, at (a) t = 100, (b) t = 500 years.

For a deeper reservoir (A = 2), **Figure 8** shows the results for the case Ra_s = 10,000 and N = 100. In this case also, the early stage behavior is same as that for A = 0.5 or 1. The 23 cells merge to form only 4 plumes after 20 years where concentrations at left walls are invariant and one front advances along the edge of the right wall. The middle three CO_2 fronts merge to only a long one as time marches. However, the plume at the right edge becomes bigger pushing others to left. Thus the dissolution accelerates, reaching 0.60 after 500 years. When the thermal effect is increased (N = 2) the long term dissolution process changes. After 100 years of simulation, plumes of various random sizes and shapes are traced. During the 500 year period only one big CO_2 front is survived, which is yet to reach the bottom. Average concentration of the aquifer at this time is 0.46. These are shown in **Figure 9**. Actually internal interactions among the fingers decrease, and the time required for CO_2 front to touch the bottom of the reservoir increases with increasing aspect ratio. These are consistent with the findings by Farajzadeh et al (Farajzadeh et al., 2007).

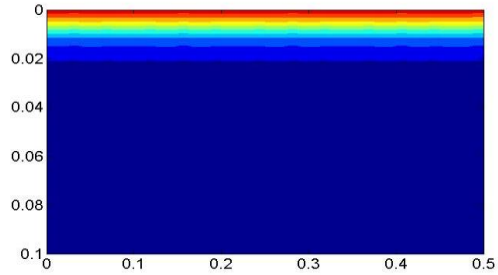

(a)

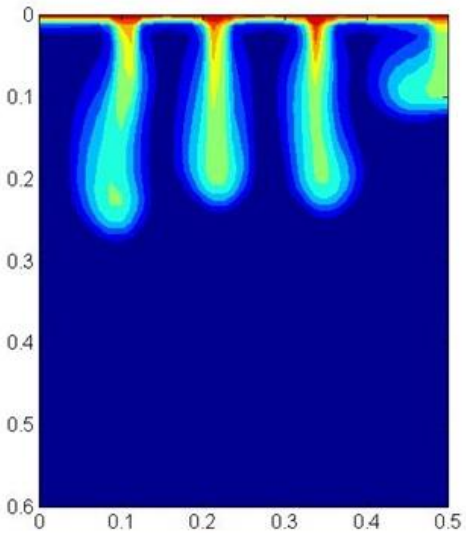

(b)

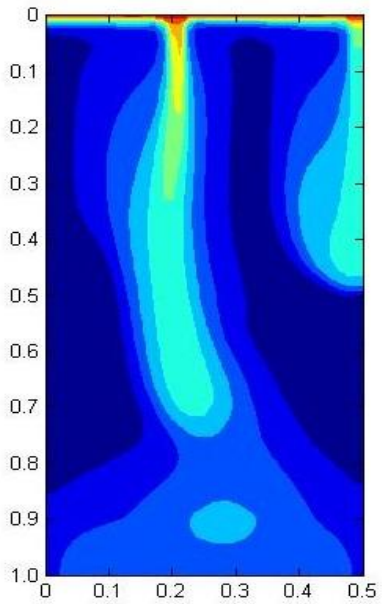

(c)

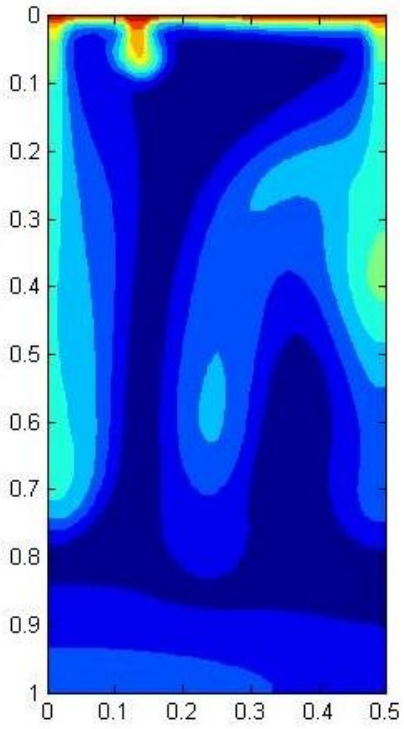

(d)

Figure 8: Concentration profiles for Ra_s = 10000, N = 100, A = 2.0, at (a) t = 4, (b) t = 20, (c) t = 100, (d) t = 500 years.

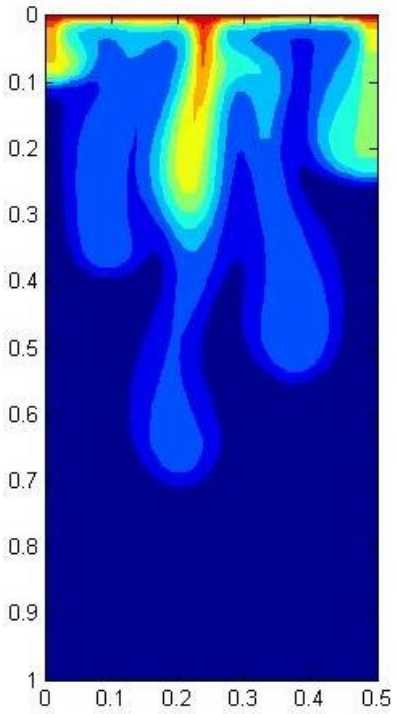

(a)

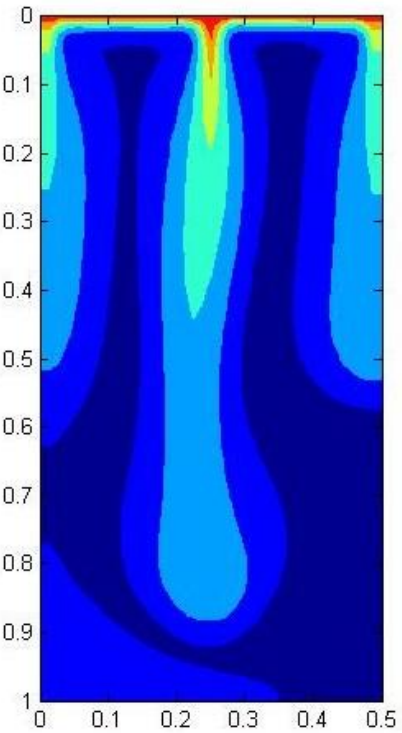

(b)

Figure 9: Concentration profiles for Ra_s = 10000, N = 2, A = 2.0, at (a) t = 100, (b) t = 500 years.

Figure 10 shows the average dissolution of CO_2 over time up to 500 years in a square

reservoir (A = 1) for various equivalent Rayleigh number, Ra_e. In early years (< 80) the average dissolution rate is faster than that at later times. Also the dissolution rate at any specific time increases with increasing Ra_e. For lower values of Ra_e, the CO_2 dissolution rate is slower because convective flow is weak and diffusion tends to dominate. To understand the behavior of the dissolution rate over a very long period, simulations were run up to 6,000 years at a fixed Ra_e of 9,900 for a square reservoir and the dissolution rate is presented in **Figure 11**. It is noted that up to about 450 years the slope is very steep. After that the rate becomes slower and after 2,000 years, the rate of dissolution becomes asymptotic to about 0.95. Primarily, every concentration finger is surrounded by thin shear layer, and as they mix together over the time the layer becomes thicker and after long time the propagation again becomes diffusion dominated. To reach complete equilibrium stage, when CO_2 concentration in the aquifer is uniform everywhere, may require thousands of years. **Figure 12** shows the effects of aspect ratios on CO_2 dissolution rate. It is observed that CO_2 dissolution rate increases slightly as the reservoir becomes laterally wide with increasing aspect ratio because fluid gets more free space to move in laterally wide reservoir enhancing the convection. Therefore from practical point of view laterally wide reservoir is better candidate than the deep aquifer for sequestration of CO_2.

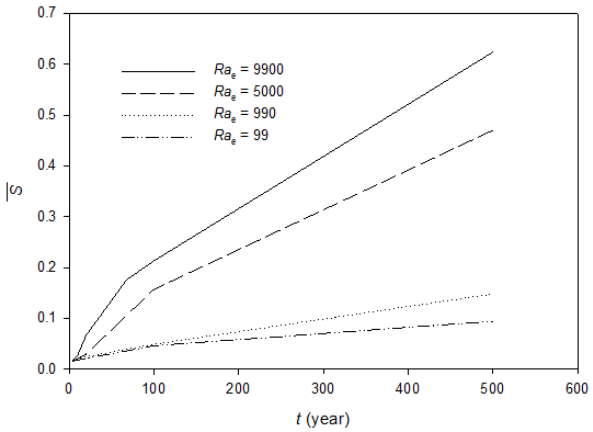

Figure 10: average dissolution over the time for different Ra_e's (A = 1).

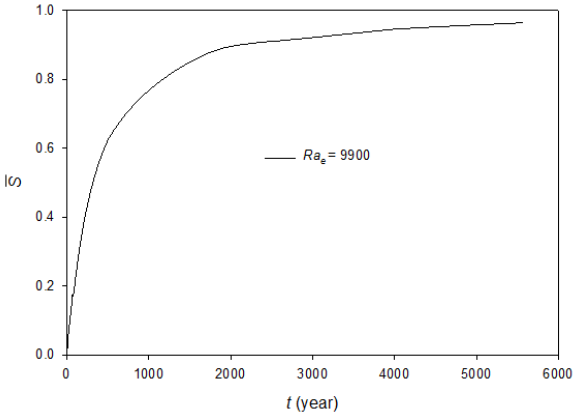

Figure 11: average dissolution over the time for different Ra_e = 9900 (A = 1).

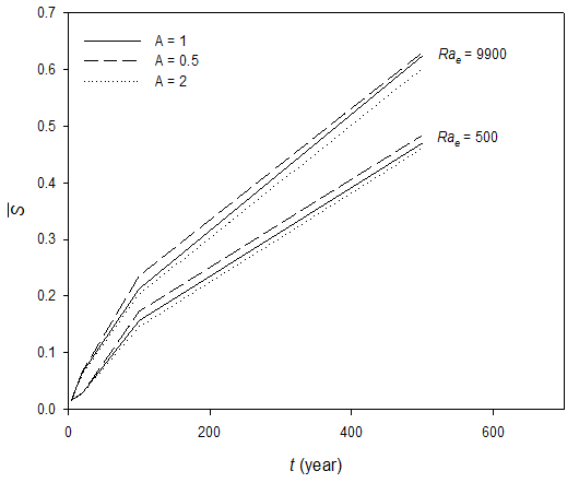

Figure 12: average dissolution over the time for different aspect ratios.

CONCLUDING REMARKS

Double diffusive natural convection in a two dimensional brine saturated porous media, subjected to vertical concentration and temperature gradients, is investigated numerically. The study is focused on the influence of the solutal and thermal buoyancy forces on the propagation of the concentration front and its resulting dissolution into the brine in the context of CO_2 sequestration in underground reservoirs. It is found that the thermal effect does not interfere the natural convection process significantly unless the buoyancy ratio, N, is low and close to one. For higher values of N (>50), the equivalent Rayleigh number, Ra_e, does not change much and the double diffusion is basically like density-driven mass transfer due to concentration variation. The convection process enhances with increasing Ra_e, which depends on reservoir characteristics and physical properties of the brine, viz., porosity, permeability, diffusivity, concentration gradient, thermal gradient, etc.

As the time passes the number of CO_2 fronts decrease due to decreasing convection process. At very initial stage (<10 years) the average CO_2 dissolution is same for all cases studied because of diffusion domination propagation. After 500 years of simulation CO_2 dissolution is over 0.60 for N = 100, and over 0.40 for N = 2. After 2,000 years the dissolution process again becomes very slow. The reservoir may be completely CO_2 saturated after thousands of years. Changing reservoir aspect ratio does not affect the average dissolution rate much, however the laterally wide reservoir is favorable than the deeper one.

NOTATIONS

A aspect ratio, H/L [-]
c concentration [mol/m^3]
C_p heat capacity at constant pressure [Jkg^{-1}K^{-1}]
D Diffusion coefficient [m^2/s]
g acceleration due to gravity [m/s^2]
H porous medium height [m]
k permeability [m^{-2}]
L porous medium length [m]
n number of nodes
p pressure [Pa]
Le Lewis number [-]
Pe Peclet number [-]
Pr Prandtl number [-]
Ra Rayleigh number [-]
$\bar{S}$ average dissolution
t time [s]
u velocity [m/s]
x distance along x-axis
z distance along z-axis

Greek letters
α thermal diffusivity
β_c coefficient of density increase by concentration [m^3/mol]
β_T coefficient of thermal expansion[K^{-1}]
φ porosity [-]
μ viscosity [kgm^{-1}s^{-1}]
κ thermal conductivity []
ρ density [kg/m^3]
ψ stream function [m^3/m^{-1}s^{-1}]

Superscript
$*$ Dimensionless quantity

Subscripts
0 initial value
c concentration
i node in x – direction
j node in z – direction
r reference value
s solutal
T Temperature
x x-coordinate
z z-coordinate

REFERENCES

Bhadauria, B.S., 2006. Temperature modulation of double diffusive convection in a horizontal fluid layer. Z. Naturforsch 61a, 335-344.

Cooper, C.A., Glass, R.J., Tyler, S.W., 1997. Experimental investigations of the stability boundary for double-diffusive finger convection in a Hele-Shaw cell. Water Resources Research 33, 517-526.

Ennis-King, J., Paterson, L., 2003. Role of convective mixing in the long-term storage of carbon dioxide in deep saline formations, SPE Annual Technical Conference and Exhibition, Denver, Colorado.

Ennis-King, J., Paterson, L., 2005. Role of convective mixing in the long-term storage of carbon dioxide in deep saline formations. SPE J.

Farajzadeh, R., Salimi, H., Zitha, P.L.J., Bruining, J., 2007. Numerical simulation of density-driven natural convection in porous media with application for CO_2 injected projects. Int. J. Heat Mass Transfer 50, 5054-5064.

Farajzadeh, R., Zitha, P.L.J., Bruining, J., 2009. Enhanced mass transfer of CO_2 into water: experiment and modeling. Ind. Eng. Chem. Res. 48, 6423-6431.

Green, T., 1984. Scales of double-diffusive fingering in porous media. Water Resources Research 20, 1225-1229.

Gunn, R.D., Krantz, W.B., 1980. Reverse combustion instabilities in tar sands and coal, pp. SPE 6735-PA.

Hassanzadeh, H., Pooladi-darvish, M., Keith, D.W., 2005a. Modeling of convective mixing in CO_2 storage. J. Can. Pet. Technol. 44, 43-51.

Hassanzadeh, H., Pooladi-darvish, M., Keith, D.W., 2005b. Scaling behavior of convective mixing, with application to geological storage of CO_2. AIChE J. 53, 1121-1131.

Islam, A.W., Carlson, E.S., 2012. Viscosity models and effects of dissolved CO2. Energy & Fuels.

Javaheri, M., Abedi, J., Hassanzadeh, H., 2010. Linear stability analysis of double-diffusive convection in porous media, with application to geological storage of CO_2. Transport in Porous Media 84, 441-456.

Landau, L.D., Lifshitz, E.M., 1969. Statistical physics: course of theoritical physics. Pergamon Press.

Lerner, K.L., Lerner, B.W., 2003. World of earth science. Gale Cengage, Farmington Hills, MI.

Lindeberg, E., Wessel-berg, D., 1997. Vertical convection in an aquifer column under a gas cap of CO_2. Energy Convers. Mgmt 38, S229-S234.

Mojtabi, M.C.C., Razi, Y.P., Mojtabi, J., 2005. Effect of vibration on the onset of double-diffusive convection in porous media, in: Ingham, D.B., Pop, I. (Eds.), Transport phenomena in porous media. Elsevier Ltd., Kidlington.

Newell, D.L., Viswanathan, H.S., Lichtner, P.C., Carey, J.W., Kaszuba, J.P., 2011. Experimental determination of supercritical CO_2 mass transfer rates into brine, American Geophysical Union, Sanfrancisco.

Oldenburg, C.M., Pruess, K., 1998. Layered thermohaline convection in hypersaline geothermal systems. Transport in Porous Media 33, 29-63.

Poulikakos, D., 1986. Double diffusive convection in a horizontal sparcely packed porous layer. Int. Comm. Heat Mass Trans. 13, 587-598.

Riaz, A., Hesse, M., Tchelepi, H.A., Orr, F.M., 2006. Onset of convection in a gravitationally unstable diffusive boundary layer in porous media. J. Fluid Mech. 548, 87-111.

Sharqawy, M.H., Lienhard V, J.H., Zubair, S.M., 2010. Thermophysical properties of seawater: a review of existing

correlations and data. Desalination and Water Treatment 16, 354-380.
Simpson, M.J., Clement, T.P., 2003. Theoritical analysis of the worthiness of Henry and Elder problems as benchmarks of density-dependent groundwater flow models. Advances in Water Resources 26, 17-31.
Sodha, M.S., Kumar, A., 1985. Stability analysis of double-diffusive solar ponds with non-constant temperature and salinity gradients. Energy Convers. Mgmt 25, 463-468.
Stern, M.E., 1975. Ocean circulation physics. Academic Press, New York.
Yortsos, Y.C., Xu, B., Salin, D., 1997. Phase diagram of fully developed drainage in porous media. Phys Rev Lett 79, 4581-4584.